Natural Biopolymer Alloys with Superior Mechanical Properties

Linghan Meng[a,‡], Fengwei Xie[,b,c,d,‡], Binjia Zhang[e], David K. Wang[f], and Long Yu[a]*

[a] Center for Polymers from Renewable Resources, School of Food Science and Engineering, South China University of Technology, Guangzhou, Guangdong 510640, China

[b] Institute of Advanced Study, University of Warwick, Coventry CV4 7HS, United Kingdom

[c] International Institute for Nanocomposites Manufacturing (IINM), WMG, University of Warwick, Coventry CV4 7AL, United Kingdom

[d] School of Chemical Engineering, The University of Queensland, Brisbane, Qld 4072, Australia

[e] Key Laboratory of Environment Correlative Dietology (Ministry of Education), College of Food Science and Technology, Huazhong Agricultural University, Wuhan, Hubei 430070, China

[f] The University of Sydney, School of Chemical and Biomolecular Engineering, Darlington, NSW 2006, Australia

Corresponding Author

* Fengwei Xie. Email: f.xie@uq.edu.au, fwhsieh@gmail.com

KEYWORDS: Chitosan; Silk peptide; Natural Biopolymers; Biopolymer alloy materials; Films; Melt processing; Mechanical properties

ABSTRACT: Natural biopolymer materials have enormous potential in important, rapidly growing applications ranging from green electronics, dye and heavy metal removal, oil/water separation, therapeutic agent delivery, tissue engineering scaffolds, biological devices, optics and sensing. However, the application of advanced functional biopolymer materials suffers from their poor processability and weak mechanical properties. Regarding this, there are enormous challenges to break the strong intermolecular interactions (hydrogen bonding) in their native forms whilst to re-establish predominant hydrogen bonding in the processed materials in a cost-effective way. Here, we report our breakthrough to prepare biopolymer alloy materials based on chitosan and silk peptide (SP) with outstanding mechanical properties via a facile, "dry", melt processing method. The 1:1 (wt./wt.) chitosan–SP film had a toughness of 19.9 J cm^{-3}, Young's modulus of 1855 MPa and tensile strength of 95.9 MPa, which are similar to, or

even better than, most engineering polymers. We propose our method could maximize the molecular interactions between chitosan and SP via a simple and effective thermomechanical mixing, which resulted in considerably enhanced mechanical properties. Moreover, dehydration/rehydration can reversibly adjust the mechanical properties of the new biopolymer alloys, which demonstrates the dominant effect of hydrogen bonding in enabling the mechanical properties of these interesting alloys. Our simple approach to engineering high-performance biopolymer materials without resorting to complex chemistries and 3D-structural construction can be envisioned to bring about a new direction in the design of advanced functional materials where cost-effectiveness is the priority.

INTRODUCTION

Natural biopolymers are highly interesting to materials scientists due to their unique properties and appealing functionality along with their abundance. For example, advanced functional materials can be made from chitosan for antimicrobial and antifungal properties,[1-5] adsorption of dyes and metals,[6-9] oleophobicity[10], electrical conductivity,[11], electroactivity,[12] and triboelectric generation,[13] which have huge potential to be applied in biomedical, environmental, energy, electronics and actuating fields. Silk fibroin (SF) is appealing in a range of applications that require a mechanically superior, biocompatible, biodegradable, and functionalizable material, such as surgical suture, tissue engineering, therapeutic agent delivery, optics and sensing.[14-20] Unfortunately, the re-processed materials based on biopolymers such as chitosan and SF traditionally exhibit poor mechanical properties due to the weak intermolecular forces, which have greatly restricted their applications. Due to this, either chitosan or SF used alone could only result in poor biological scaffolds.[21-27]

While it is challenging to re-process biopolymers into mechanically strong materials, naturally existing biopolymer materials present striking mechanical properties. For

example, the Young's modulus of chitin nanofibers is more than 150 GPa.[28] Naturally produced SF fiber (*Bombyx mori*) has an ultimate tensile strength of 300–740 MPa and a Young's modulus of 10−17 GPa.[14] Moreover, chitin and SF exist widely in natural materials such as spider silk, insect skins and nacre, which have long intrigued scientists due to their superior strength and toughness combined with stiffness or flexibility. This is the main reason that the design of strong advanced materials has largely relied on biomimetism and bioinspiration.[29-32] Research has been focused on creating sophisticated, mechanically strong biomimetic materials based on chitosan and SF with the goal to maximize the hydrogen-bonding interactions between the two biopolymers.[33-34] In particular, biomimetic laminates were achieved by layer-by-layer techniques, of which the fabrication process was time-consuming and solvent-intensive.[33-34] Therefore, in order to unleash the vast potentials of natural biopolymers, it is highly important to develop techniques that can produce materials with superior properties and also industrially scalable.

Indeed, the gridlock in the facile processing of these biopolymers has largely impeded the development of advanced functional materials based biopolymers. While the strong

intermolecular interactions (via hydrogen bonding) in the native form of biopolymers accounts for their strong mechanical properties, these interactions also make them resistant to dissolution and plasticization,[35] and thus processing. As a result, solution methods were used in most of the studies to synthesize biopolymer materials.[25, 33-34, 36-41] These methods usually require large amounts of chemicals/organic solvents and are processing time-intensive, which makes them almost impossible for scale-up production. On the other hand, effective processing should also facilitate the re-establishment of hydrogen bonding in biopolymers, by which strong mechanical properties can result.

Other than replicating the structures of biological materials, there could be alternative ways to create super strong biopolymer materials containing engineered hydrogen bonding at the molecular level.[20, 42-43] High-strength metal alloys could be achieved by dual phase nanostructuring.[44] For polymer materials, chemical reactions enable structural manipulation to achieve strong inter-/intramolecular or interfacial interactions (typically covalent bonding).[43, 45-48] We hypothesized that biopolymer alloys with strong mechanical properties could be obtained by maximizing the molecular interactions

between chitosan and protein in a well-mixed system. In this work, we adopted an innovative, facile, “dry” approach to engineering such biopolymer alloys, which resulted in a homogeneous, well-dispersed structure yet still achieved outstanding mechanical properties. Our method here is based on high-viscosity polymer melt processing, which allows a straightforward and high-efficient mixing of two different biopolymer phases. The materials were realized simply by capitalizing on electrostatic complexation of chitosan with silk peptide (SP). While protein–polysaccharide anionic–cationic complexes were always prepared in aqueous solutions,[49-51] to the best of our knowledge, this is the first attempt to construct such complexes by high-viscosity melt processing. We found that the chitosan–SP alloy films prepared by this method offered outstanding mechanical properties, which were similar to, or even higher than, those of chitosan–SF biomimetic laminates[33] and chitosan-based nanocomposites.[52] Our successful example of high-performance chitosan–SP alloys with molecularly complexed structure and exceptional mechanical properties could provide alternative solutions to traditional biomimetism for designing advanced biopolymer-based materials.

EXPERIMENTAL SECTION

Materials. Chitosan (poly(β-(1,4)-D-glucosamine), derived from crustaceous shells, with a specification of BR and low viscosity of 100 mPa·s), was purchased from Shanghai Ryon Biological Technology Co., Ltd. (Shanghai, China). This chitosan has a molecular weight of about 150,000 g mol^{-1}, a degree of deacetylation of >90%, and a viscosity of about 100 mPa·s (1% solution in 1% acetic acid at 25°C). It had an original moisture content of 10.3 wt.% measured by weight loss during drying. This chitosan has negligible solubility in water. Silk peptide (SP) powder was supplied by Huzhou Xintiansi Bio-tech Co., Ltd. (Huzhou, China). This is a water-soluble polypeptide by the degradation of silk fibroin (*Bombyx mori*) and has a molecular weight of 500–30,000 g mol^{-1}.

Glycerol, of 99.5% purity, was purchased from Sigma–Aldrich (Shanghai, China). Formic acid of 98 wt.% purity was acquired from Jiangsu Qiangsheng Chemical Co., Ltd. (Changshu, China) and used as received. Methanol was supplied by Guangzhou Donghong Industrial Development Co., Ltd. (Guangzhou, China). Sodium hydroxide

was supplied by Guangzhou Chemical Reagent Factory (Guangzhou, China). All these chemicals are of analytical grade and used as received without further treatment.

Sample Preparation. Different samples were prepared with their formulations, with their codes shown in **Table 1**. Chitosan and SP in different ratios (7:3, 6:4, 5:5, 4:6 and 3:7) were pre-blended by mechanical stirring for 15 min. During pre-blending, formic acid (60 wt.% based on the total weight of chitosan and fibroin) and glycerol (30 wt.% based on the total weight of chitosan and fibroin) were added dropwise. Then, the mixtures were stored hermetically for at least 48 h at room temperature before thermal mixing using a HAAKE Rheomix 600p two-rotor batch mixer driven by a HAAKE Rheocord Polylab RC500p system (ThermoHaake, Germany). To prevent the loss of moisture and formic acid during thermal mixing, polytetrafluoroethylene (PTFE) glass fabric was used to seal the gaps between the three barrels of the mixer and a silicon-rubber cover was used to seal the feeder on the top. **Figure S1** shows the photos of different formulations before thermal mixing.

Table 1. Sample codes and composition.

Sample	Chitosan [g]	Silk peptide [g]	Formic acid [mL]	Glycerol [mL]
C10S0	100	0	60	0
C7S3	70	30	60	0
C7S3-G	70	30	60	30
C6S4	60	40	60	0
C6S4-G	60	40	60	30
C5S5	50	50	60	0
C5S5-G	50	50	60	30
C4S6	40	60	60	0
C4S6-G	40	60	60	30
C3S7	30	70	60	0
C3S7-G	30	70	60	30
C0S10	0	100	60	0

The thermal processing was carried out at a screw speed of 20 rpm and a temperature of 80 °C for 20 min, which was determined by a stabilized torque value (see **Figure S2**). After that, the thermally processed materials were immediately hot-

pressed into films using a flat sulfuration machine (Guangzhou Shunchuang Rubber Machinery Factory, Guangzhou, China). The mold used for hot pressing consists of three stainless steel plates with the middle one containing a hollow, molding space of 100 mm × 100 mm × 1 mm in dimension. PTFE glass fabric was placed between the sample and the mold. The conditions used for hot pressing were 80 °C at 1000 bar for 3 min, followed by cooling to room temperature and maintained for 3 min. Then, the hot-pressed films were soaked in methanol for two days, and then in 4% (w/v) sodium hydroxide solution (pH = 13.60 ± 0.04) for another one day, before thoroughly washed with distilled water to remove the residual chemicals. Our observation indicated that, without the treatment with NaOH solution, the materials with high integrity and strong mechanical properties could not be obtained.

The obtained sheets were cut into dumbbell-shaped specimens. All the sample specimens were then dried in an oven at 60 °C for 2 days, and then immediately stored in a desiccator maintained at 57% relative humidity (RH) (achieved using saturated sodium bromide) for 3 weeks before characterization. In the desiccator, methylbenzene was introduced to prevent the samples from becoming moldy.

For comparison purposes, chitosan and SP, respectively, were also treated following the same procedure except conditioning, which were coded as 'C10S0' and 'C0S10'. However, C0S10 (pure fibroin), after mixed with formic acid, became a liquid that was too thin for the thermal processing. In addition, C10S0 could not be successfully processed into cohesive film using our method here due to its low plasticity.

Tensile Testing. The dumbbell-shaped specimens, corresponding to Type 4 of the Australian Standard AS 1683:11 (ISO 37:1994), were cut from the hot-pressed samples. The testing section of the specimen was 12 mm in length and 2 mm in width. Tensile tests were performed at 25 °C (room temperature) with an Instron® 5566 universal testing machine with a 100N load cell (accuracy less than ±1% of the indicated value) at a constant crosshead speed of 3 mm/min. As the specimens were in the form of thin sheeting, specimen extension was measured by grip separation as suggested by ASTM Standard D882. Young's modulus (E), tensile strength (σ_t), and elongation at break (ε_b) were automatically determined by the Instron® Merlin software from at least 7 specimens for each sample (specimens that failed at some obvious flaw or that failed at the jaw were not included). Toughness (U_T), or tensile energy to break (TEB), was

calculated by integrating the energy absorbed per unit volume under the stress–strain curve.

Fourier-transform Infrared (FTIR) Spectroscopy. A PerkinElmer Spectrum 100 FT-IR spectrometer, fitted with a universal ATR accessory, was used to collect infrared spectra of the samples. The spectra were recorded over the range of 4000–650 cm^{-1} with a resolution of 4 cm^{-1} and 64 scans, and were baseline-corrected using the Spectrum software before analysis.

Thermogravimetric Analysis (TGA). A PerkinElmer Diamond thermogravimetric analysis (TGA) facility was used to determine the decomposition temperatures of samples by a temperature ramp from 30 °C to 550 °C at 5 °C/min in a nitrogen atmosphere. For each measurement, about 3 mg of the sample was weighed into a platinum pan, which was then mounted onto the TGA facility. The degradation temperature was determined from the peak temperature of the derivative weight loss curve.

Dynamic Mechanical Thermal Analysis (DMTA). A PerkinElmer Pyris Diamond DMTA with a single cantilever tensile mode was used to evaluate the dynamic mechanical

properties of the films as rectangular tensile bars. The length of the tested tensile section was 20 mm. The tests were carried out at a frequency of 1 Hz, a temperature between −100 °C and 120 °C, a heating rate of 2 °C/min, and a strain of 0.05%. The dynamic storage modulus (E'), loss modulus (E''), and loss tangent ($\tan \delta = E''/E'$) were obtained from the tests. To prevent water evaporation during the tests, the specimens were coated with Vaseline grease. No swelling of the specimens was observed, suggesting no adverse effect of Vaseline.

X-ray Diffraction (XRD). X-ray diffraction (XRD) with an Xpert PRO diffractometer (Bruker, Germany) was performed on the conditioned chitosan/fibroin sheets operating at 40 mA and 40 kV and using Cu K radiation with a wavelength of 0.15418 nm as the X-ray source. The scanning of diffraction angle (2θ) was from 4° to 50° with a scanning speed of 2 s/step and a scanning step of 0.02°.

Scanning Electron Microscope (SEM). The conditioned chitosan/fibroin blends were cryo-fractured in liquid nitrogen, fixed on a sample stub and then gold coated to a 5 nm thickness using an Eiko Sputter Coater, under vacuum. The sectional morphology of the

blends samples was examined using an EVO18 scanning electron microscope (ZEISS, Oberkochen, Germany) operated at a voltage of 10.0 kV.

Water Uptake (UP). The samples after conditioned for 3 weeks (dry samples) were weighed firstly. For water uptake measurements, the samples were soaked in distilled water at 37 °C and the swollen samples were weighted after removing the excess water. The water update (WU) ratio was calculated using the following equation:

$$WU\% = \frac{W_s - W_d}{W_d} \times 100\% \quad (1)$$

where W_s is the weight of the swollen samples (g) and W_d is the weight of the dry samples (g).

RESULTS AND DISCUSSION

Preparation and Mechanical Properties. **Figure 1** shows our simple procedure for preparing biopolymer alloy films. Chitosan and SP were blended together with the addition of formic acid, which was then thermomechanically kneaded at 80 °C for

20 min to ensure adequate mixing (as seen from the stabilized torque values, **Figure S2**), followed by hot pressing to obtain the films. After alcohol and alkali treatments, the films were cut into dumbbell bars (**Figure S1**). We studied both the effects of chitosan/SP ratio and the addition of glycerol as a plasticizer. As an example, the sample names are coded as “C6S4-G” which means the chitosan (C) / SP (S) ratio was 6:4 and “G” means that the formulation was added with 30 wt.% of glycerol based on the total weight of chitosan and SP. These dumbbell bars were tested for mechanical properties either immediately (still in the hydrated state, denoted by “W”) or after oven drying and conditioning at 57% relative humidity for 3 weeks. While oven drying could remove all the free water from the films, all the conditioned materials contained only about 6–8% moisture content (**Figure S3**).

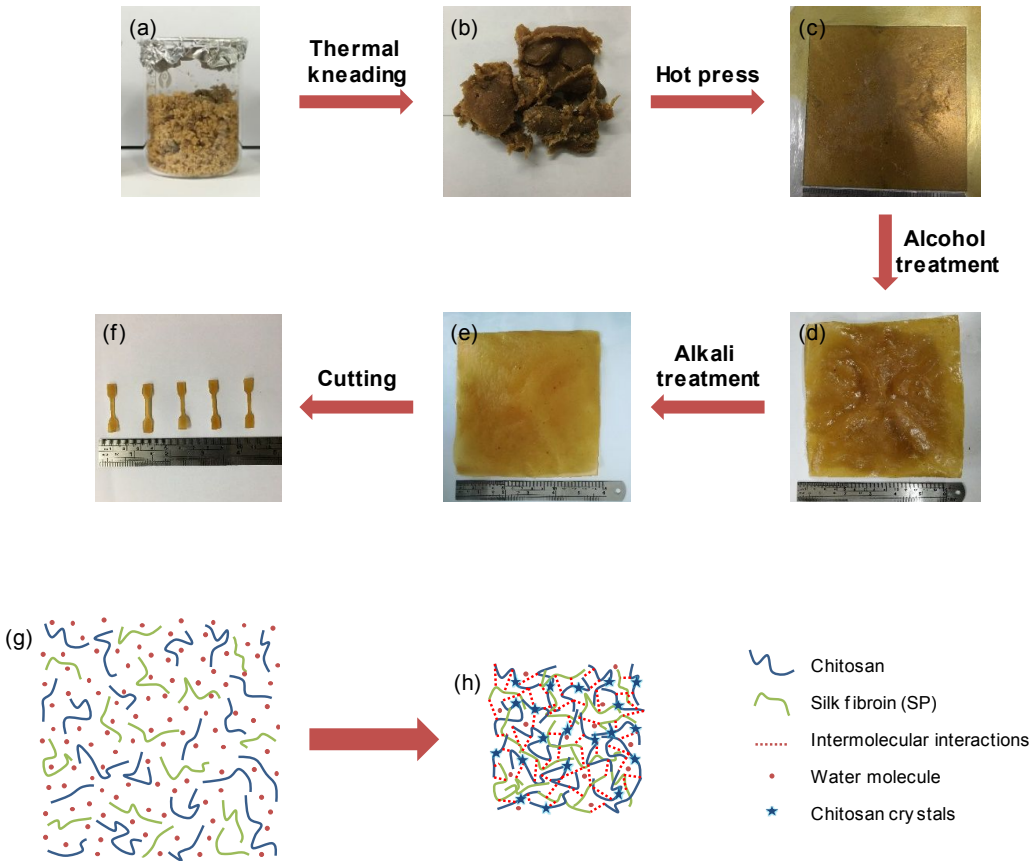

Figure 1. Preparation of biopolymer alloy films. a) 5:5 (wt./wt.) chitosan/SP blend with 60 wt.% formic acid; b) the sample after thermomechanical kneading at 80 °C for 20 min; c) after hot pressing at 80 °C; d) after treatment with methanol for two days; e) after treatment with NaOH solution for one day; f) after washed with water and cut into dumbbell bars; g) schematic corresponding to a; f) schematic corresponding to e or f.

Figure 2 shows the mechanical properties of the different chitosan–SP alloy films. Overall, there were significant differences in tensile strength (σ), Young's modulus (E), elongation at break (ε_b), and toughness (U_T) between the samples before conditioning (as wet samples (W)), after conditioning, and further after rehydration (W2 samples). For all the formulations, the ε_b was decreased by conditioning, which is expected due to the largely reduced moisture content in the samples. For example, the ε_b of C5S5 (W) was 115.2%, which was reduced to 26.2% after conditioning. Nonetheless, σ, E, and U_T were remarkably increased by conditioning. For C5S5 (W), for example, the σ, E, and U_T were 3.0 MPa, 3.1 MPa and 2.4 J/cm^{-3}, respectively, which were drastically increased to 95.9 MPa (32 times), 1855 MPa (580 times), and 19.9 J/cm^{-3} (8.3 times) respectively after conditioning. The extraordinary mechanical properties of these biopolymer alloys are comparable to most engineering polymers and many metals and composites. A long-standing challenge in engineering material design is the trade-off between strength and toughness because these properties are generally mutually exclusive.[53-54] However, our biopolymer alloy materials overcame this trade-off as evidenced by both dramatically increased σ and U_T. Moreover, our biopolymer alloys

present mechanical properties that are much stronger than chitosan-based materials and nanocomposites,[52] and even better than chitosan–fibroin biomimetic laminates.[55]

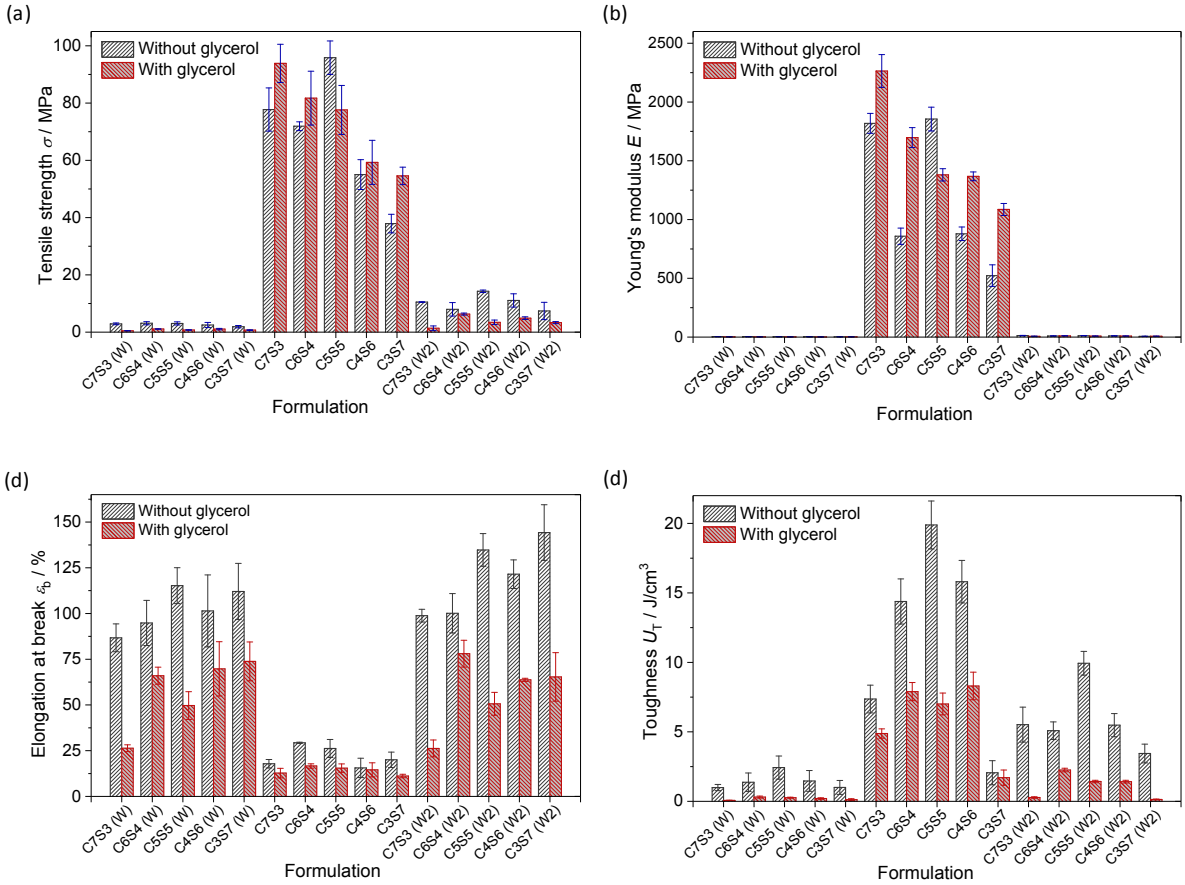

Figure 2. Mechanical properties of biopolymer alloys of different chitosan/SP ratios. a) Tensile strength; b) Young's modulus; c) Elongation at break; d) Toughness. Regarding the suffix to the sample code, "W" means the wet samples that were freshly prepared

(before oven drying and conditioning); “C”, the conditioned samples (after oven drying and conditioning); and “W2”, the samples after further being soaked in water for 30 min.

We propose that high-viscosity thermomechanical mixing along with conditioning enhanced the interactions between biopolymer chains and allowed significant molecular chain rearrangements. This conjecture is principally the reason that our chitosan–SP biopolymer alloys produced excellent mechanical properties. Similarly, recent work[42, 56] has shown that with the enhanced hydrogen bonding between cellulose molecular chains, densified bulk natural wood displayed more than a tenfold increase in strength, toughness and ballistic resistance and with greater dimensional stability. Here, the change in internal interactions for the samples can also be seen from the tensile stress–strain curves (**Figure S4**). For W samples, there was a linear relationship between stress and strain, which is typical of an elastomeric polymer (and is expected for the moisture-saturated biopolymer materials here). The stress–strain curve after

conditioning is typical of a hard and tough polymer, with strain hardening observed, which demonstrate the strong interactions between biopolymer chains.

To further check if rehydration would influence the hydrogen bonds in biopolymer alloys, we also tested the mechanical properties of the biopolymer alloy films that were further immersed in water for 30 min (denoted by "W2"). 30 min of immersion was shown to be enough for the alloy films to achieve a well-saturated state in water (**Figure S5**). The results in **Figure 2** shows that rehydrated samples (W2) displayed mechanical properties that were mostly reversed back to its virgin wet state (W) (except that the toughness for W2 was still marginally higher than that for W). Regarding this, the water molecules in W2 samples might have disrupted most of the intermolecular hydrogen bonding in the films by interacting with the hydroxyl groups of biopolymers. This loss of hydrogen bonding between biopolymer chains can also be evident by the linear tensile stress–strain curves (**Figure S4c**). The results here demonstrate the reversible mechanical properties of biopolymer alloy materials that can be well controlled by an external hydrogen-bonding breaker (for example, water here). Moreover, biopolymer alloy materials showed enlarged dimensions upon hydration (W2), which were

measured over 80% of the original dimensions of W samples (**Figure S6**), while the integrity of the films was still kept. The materials tend to maintain a sponge-like structure with interconnected polymer chains probably reinforced by chitosan crystals (**Figure 1g**, **1h**, and **4**; further discussed later). These features could allow this new type of material to be highly useful for application as artificial skins and wound dressings.

We propose that the enhanced mechanical properties are attributed to both the strong intermolecular electrostatic interactions and intermolecular hydrogen bonding between the two polysaccharides.[40, 57] In addition to increasing intermolecular hydrogen bonding between chitosan and SF,[25, 37-39] electrostatic complexation of chitosan and SP also play a more important role in the biphasic interactions of dissimilar biopolymers. The effect has also been shown to enhance material strength and durability.[58] At low pH with the treatment of formic acid, the amino groups of both chitosan and SP were protonated and positively charged, causing electrostatic repulsion between the polymer chains and thus enabling polymer solvation. Considering the rather low isoelectric point of SP (< pH 2.8)[59] (also **Figure S7**), the increased pH with NaOH treatment would make SP become negatively charged, and thus induced electrostatic interactions with the positively

charged chitosan. The electrostatic complexation could be responsible for the high degree of miscibility between chitosan and SP as determined by their morphology (discussed later by SEM) and result in excellent physical properties.[58] This complexation would then facilitate the strong hydrogen bonding interactions between biopolymer chains in a later stage as illustrated in **Figure 1**.

From **Figure 2**, we can see that C6S4, C5S5, and C4S6 showed the best mechanical properties (σ, E, and U_T) after conditioning. For these formulations, the addition of glycerol had a different effect on σ and E. Regarding this, glycerol, usually function as a plasticizer, may increase the biopolymer chain mobility to allow a favorable chain rearrangement. Meanwhile, glycerol tends to interact with biopolymers via hydrogen bonding and thus may interfere with the interactions between biopolymer chains. Moreover, SP may also have some plasticization effect on chitosan. The formulations with a higher SP content were more liquid-like before processing (**Figure S1**). The plasticization effect could be shown by the reduced σ, E, and U_T of C4S6 and further of C3S7. Another reason for the inferior mechanical properties of higher-SP-content samples is that the most electrostatic complexation between chitosan and SP could only

be achieved with the matched numbers of anionic groups of SP and cationic groups of chitosan,[58] leading to maximized hydrogen bonding interactions and thus mostly enhanced material performance.

We could not successfully prepare films based on only chitosan or fibroin using the same procedure. Fibroin was a liquid state after the same treatment (**Figure S1**). In contrast, chitosan alone was found to be lacking plasticization and thus integral films based on only chitosan could not be formed by hot pressing.

Morphology. **Figure 3** shows the SEM images of the cryogenically fractured surfaces of the different chitosan–SP alloy films after conditioning. It can be seen that all the samples showed a relatively smooth, non-porous fractured surface. This morphology indicates the excellent plasticization and mixing of the materials. Besides, the SEM images could not show any discernible phase separation between chitosan and SP, indicating excellent miscibility between the two biopolymers irrespective of the concentration, which suggests the strong intermolecular electrostatic interactions and intermolecular hydrogen bonding between the two polysaccharides.

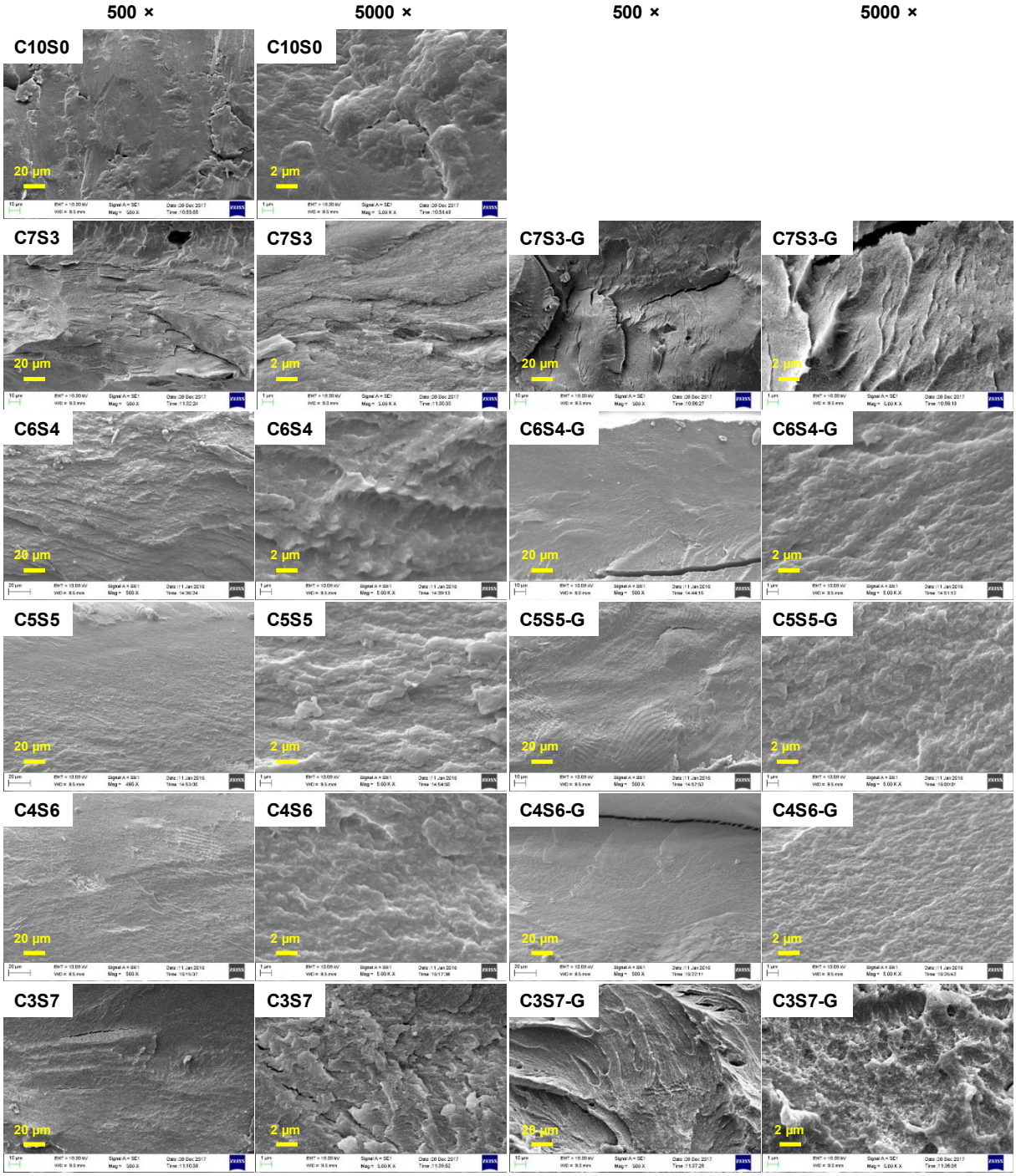
500 ×
5000 ×
500 ×
5000 ×
C10S0
20 µm
C10S0
2 µm
C7S3
20 µm
C7S3
2 µm
C7S3-G
20 µm
C7S3-G
2 µm
C6S4
20 µm
C6S4
2 µm
C6S4-G
20 µm
C6S4-G
2 µm
C5S5
20 µm
C5S5
2 µm
C5S5-G
20 µm
C5S5-G
2 µm
C4S6
20 µm
C4S6
2 µm
C4S6-G
20 µm
C4S6-G
2 µm
C3S7
20 µm
C3S7
2 µm
C3S7-G
20 µm
C3S7-G
2 µm

Figure 3. SEM images of biopolymer alloy films of different chitosan/SP ratios after oven drying and conditioning.

Usually, biopolymer blends without strong intermolecular bonding between the phases would generally lead to increased porosity upon dehydration.[60] However, no macroscopic pores were observed in all these conditioned samples although some moisture was expected to be transferred throughout the material and evaporated during oven drying at 60 °C. It is suggested that the chitosan–SP alloy contracted uniformly as a whole upon dehydration due to the strong, homogeneous interactions throughout the material. This dimensional change was also confirmed by the shrinkage of the materials after oven drying (56–73% of their original dimensions, see **Figure S6**).

X-ray Diffraction (XRD). Using XRD, we examined the crystalline structure of raw chitosan and SP and different chitosan–SP alloy films (**Figure 4**). Raw chitosan displayed two major peaks at 2θ of about 10° and 20°.[61-62] The peak at 10° 2θ (020

reflection) is assigned to the hydrated crystals due to the integration of water molecules in the crystal lattice and the peaks located at 20° 2θ (100 reflection) is attributed to the regular crystal lattice of chitosan.[63] After the raw chitosan was treated with formic acid and thermally processed, the C10S0 sample (W) displayed a different XRD pattern — the original peaks at 10° 2θ and 20° 2θ became unapparent and a broad amorphous halo centered around 23° 2θ was shown, indicating a predominantly amorphous structure. On the other hand, raw SP displayed a broad amorphous halo centered at 22° 2θ, suggesting a mostly amorphous structure. A typical β-sheet structure of crystalline silk could not be observed here.[64-65]

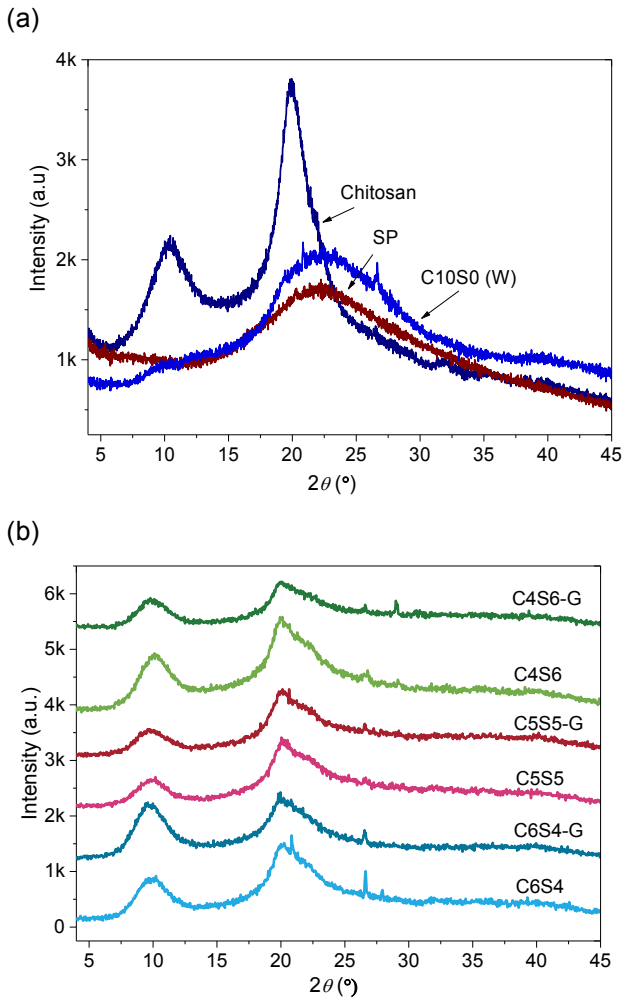

Figure 4. XRD patterns of a) raw chitosan, raw SP, and C10S0 (W) (the processed chitosan without oven drying and conditioning); and b) biopolymer alloy films of different chitosan/SP ratios after oven drying and conditioning.

In **Figure 4b**, it can be seen that all the chitosan–SP alloy films after conditioning showed very similar XRD patterns with two apparent peaks at 2θ of about 10° and 20° as similarly shown for the raw chitosan. All of these alloy films displayed some degree of crystallinity, which was enabled by conditioning, given that C10S0 (W) was mostly amorphous (**Figure 4a**). Conditioning would facilitate the hydrogen-bonding interactions between chitosan, SP, water and glycerol, and the rearrangement of chitosan molecular chains. The electrostatic complexation and hydrogen bonding might have assisted chitosan crystallization as well. The intensities of the characteristic peaks were inferior to those of raw chitosan, suggesting much lower degrees of crystallinity of chitosan that was induced by conditioning.

Figure 4b also indicates that the different chitosan–SP alloy films had slightly different degrees of intensity of the peaks. It can be seen that the samples with a lower content of chitosan (or a higher content of SP) exhibited slightly weaker peaks. However, it is surprising to see that C4S6 displayed stronger XRD patterns than C5S5 and C5S5-G. Regarding this, the treated SP might have facilitated the movement of chitosan chains and the crystallization of chitosan. This observed effect of SP here disagrees with the

well-recognized view that, in the disorganized composite materials, the addition of fibroin interferes with this crystallization process of chitin/chitosan and thereby decreases the mechanical strength of chitin/chitosan.[33] This suggestion is based on the theory that the nitrogen atom in the number 2 position of the chitosan ring mediates either interchain bonding within its crystal forms or its bonding to fibroin.[33]

In contrast to SP, glycerol seemed to have a counter effect on the crystallization of chitosan as C4S6-G displayed less intensive peaks compared with C4S6. There has been no consistent conclusion regarding the effect of glycerol on the crystallinity of chitosan-based materials.[52, 61-62] Glycerol may favor the chain mobility and thus enables the chitosan crystallization process,[52, 61] while a higher content of glycerol could suppress the crystallization of chitosan as well.[52, 62]

Fourier-transform Infrared (FTIR) Analysis. FTIR analysis was undertaken to understand the chemical interactions in chitosan–SP alloy films (**Figure 5**). For all the samples, a broad peak from 3600 cm^{-1} to 3100 cm^{-1} was shown, which corresponds to the –OH stretching and bending vibration mode in the molecule.[66] In **Figure 5a**, the raw chitosan showed absorption bands at 1149 cm^{-1} and 895 cm^{-1}, which are attributed to

the saccharide structure.[36, 38] The intense absorption bands at 1065 cm^{-1} and 1028 cm^{-1} is due to the -C-O- ether stretching vibration involving the glucosamine skeleton.[21, 38] The raw chitosan also showed absorption bands at 1651 cm^{-1}, 1585 cm^{-1}, and 1260 cm^{-1}, which are ascribed to amide I, amide II, and amide III, respectively.[25, 33, 39, 66-67] Amide I is primarily governed by mostly the C=O stretching vibration and secondarily the C-N stretching vibration. Amide II derives from mainly in-plane N-H bending and secondarily the stretching vibration of C-N and C-C stretching vibrations. The absorption band at 1585 cm^{-1} is also assigned to the amino group of chitosan.[37] For the raw chitosan, there was also an absorption band at 1377 cm^{-1}, which is assigned to the CH_3 symmetrical deformation mode.[67] The existence of amide groups is consistent with the incomplete deacetylation of chitin. For the processed chitosan (C10S0), all these groups are maintained. The band representing amide II also shifted to a lower frequency. This band signal may also have a contribution from amine I (N–H bending from the amine and acetylamine) and C–N stretching modes.[33] These results suggest that there could be increased hydrogen-bonding interactions involving these groups in the processed chitosan.

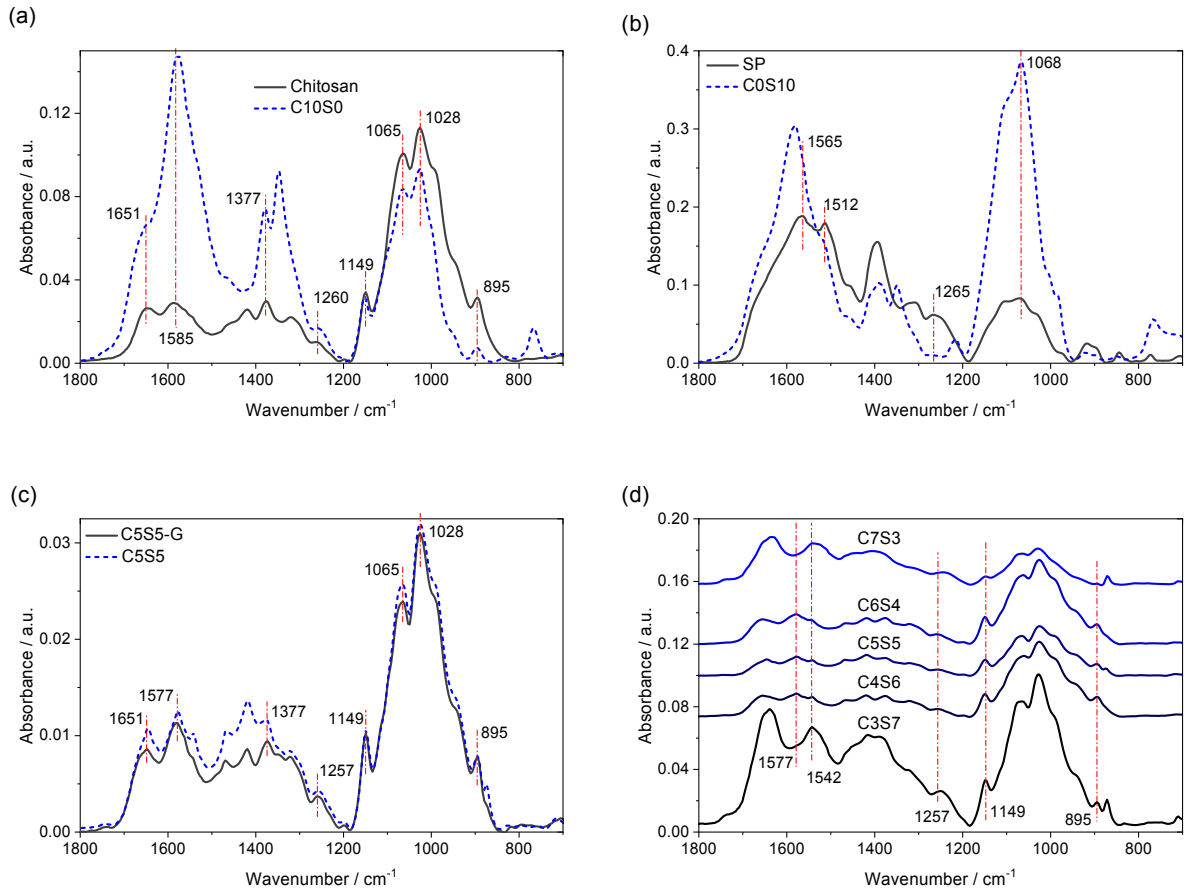

Figure 5. FTIR spectra for a) raw chitosan and C10S0 (dried); b) raw SP and C0S10 (dried); c) and d) biopolymer alloy films of different chitosan/SP ratios after oven drying and conditioning.

In **Figure 5b**, the raw SP shows absorption bands at 1565 cm^{-1} and 1512 cm^{-1} (amide II), 1265 cm^{-1} (amide III), and 1068 cm^{-1} (amide IV). All these peaks are attributed to a random coil structure,[21, 36, 40, 68-69] and suggest that the raw SP composed of an amorphous structure. For the treated SP (C0S10), the vibrational bands for amide II shifted to a higher wavenumber. Therefore, it could be suggested that the chemical treatment and thermal processing resulted in interactions between these amide groups, most likely through hydrogen bonding. However, no absorption bands that are characteristic of β-molecular conformation are evident in the spectrum.[40, 68-71]

From **Figure 5c**, it can be seen that the absorption bands of C5S5 and C5S5-G are highly similar, which suggests that glycerol did not cause a pronounced effect on the chemical interactions. Besides, the absorption bands of C5S5 and C5S5-G matched quite well with that of chitosan alone (**Figure 5a**), and the characteristic bands of SP were not evidence. This is possibly relating to the characteristic amide bands of SP, which overlap those of chitosan, suggesting strong interactions between SP and chitosan. Similar reports showed that the intermolecular interactions among biopolymers could be associated with the amide groups of SP and C=O and amino

groups of chitosan through hydrogen bonding [25, 37-39]. Comparing **Figure 5c** with **Figure 5a**, it can be noted that there was a shift of the amide II band signal to lower wavenumbers (from 1585 cm^{-1} to 1577 cm^{-1}).[33, 38] The FTIR results indicate that there may be increased hydrogen-bonding interactions involving these groups in the processed chitosan. Interestingly, this shift of the amide II band signal was much more pronounced for C7S3 and C3S7 (**Figure 5d**), suggesting even stronger interactions.

Dynamic Mechanical Thermal Analysis (DMTA). DMTA was used to investigate the relaxation temperatures of the different chitosan–SP alloy films (**Figure 6**). For all the samples, an apparent transition between −60 °C and −10 °C can be identified. The peak at this low-temperature region, indicating β-relaxation, has been attributed to the motions of the side chains or lateral groups of chitosan interacting with small molecules of water and/or glycerol by hydrogen bonding.[52, 72-73] Similarly, as the transition between −60 °C and −10 °C occurred for all the samples, this transition was probably due to the motions of the side chains or lateral groups of chitosan interacting with low-molecular-weight substances such as water and SP by electrostatic interaction or hydrogen bonding, irrespective of glycerol. It can be seen from **Figure 6** that there are no apparent

differences in this transition temperature among different formulations. Nevertheless, the intensity of this transition was slightly higher when the chitosan content was higher.

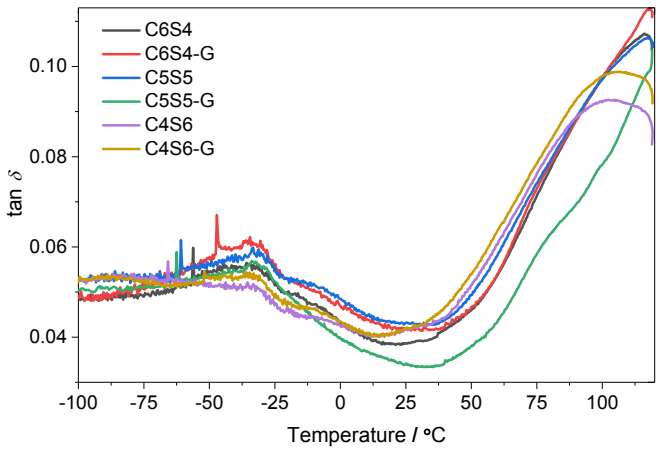

Figure 6. DMTA curves for biopolymer alloy films of different chitosan/SP ratios after oven drying and conditioning.

On the other hand, with the increased temperature from about 30 °C, the tan δ rapidly increased to form another peak between 110 to 140 °C (**Figure 6**). This peak at the

higher temperature range could be related to the α relaxation, which can be linked to the glass transition (T_g) of the chitosan.[72-73] Our biopolymer alloys show a T_g higher than chitosan-based materials reported before.[52, 61, 72-73] The motion of chitosan chains probably was restricted by the intermolecular chain interaction with SP, which might be the cause of the high T_g. Such a rigid structure of the amorphous material in chitosan–SP alloy films is well correlated to the high stiffness and low ε_b as discussed before.

Thermogravimetric Analysis. The thermal stability of different chitosan–SP alloy films was studied by TGA with a temperature scan up to 550 °C, which is shown by the way of derivative weight loss (**Figure 7** and **Table S1**). For the raw chitosan, there was a large thermal decomposition peak spanning from about 200 °C to 400 °C, with a peak temperature at 301 °C. This result for chitosan is in agreement with previous studies.[52, 62] The raw SP displayed a broad thermal decomposition peak starting from about 150 °C and ending at 470 °C, with a peak temperature at 232 °C. A single decomposition step was also reported for *Bombyx mori* SF.[74-75] However, the peak temperature of SP was lower than that (about 300 °C) of SF,[74] which could be due to

the difference in their molecular weights. The TGA of glycerol was also undertaken, which showed a sharp peak at 232 °C.

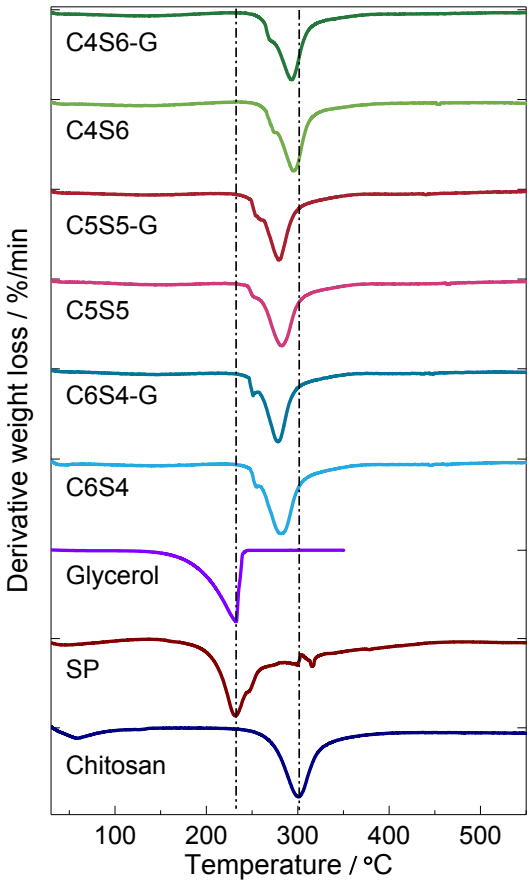

Figure 7. Derivative weight loss curves for raw chitosan, raw SP, glycerol, and biopolymer alloy films of different chitosan/SP ratios after oven drying and conditioning.

Representative chitosan–SP alloy samples with similar derivative-weight-loss profiles are shown in **Figure 7**. A large peak spanning a temperature range of 280–296 °C overlaps another smaller peak at 254–271 °C. The peak at the lower temperature is considered to be associated with SP and glycerol, and the larger peak at the higher temperature is attributed to chitosan. We can note from the weight-loss profiles that for all the alloy samples, the peak temperature for the SP component is observed to be higher than that for the raw SP while the peak temperature for chitosan is lower than that for the raw chitosan. The fact that their corresponding peak temperatures shifted closer to one another clearly indicates that there were strong physicochemical interactions between chitosan and SPin the system. Moreover, the two peak temperatures for our chitosan–SP alloy films are found to be higher than those for chitosan–fibroin blend films reported elsewhere.[25, 55] The higher thermal stability corresponds to the strong intermolecular chain interactions and the rigid and dense structure embedded with chitosan crystals in chitosan–SP alloy films. Moreover, **Table**

S1 shows that the effect of glycerol on the thermal decomposition temperatures was minor.

CONCLUSION

There has been an on-going challenge of producing the advanced biopolymer materials with cost-effective, industrially relevant techniques whilst improving the mechanical properties. This work demonstrates that a new type of biopolymer alloy materials with astonishing mechanical properties can be prepared by an innovative, facile method involving high-viscosity melt processing enabling effective mixing of the two biopolymers. As our biopolymer alloy films contained no distinct 3D-designed or patterned phase structure that is widely pursued by high-performance polymer materials, the superior mechanical performance of these alloy materials are totally unexpected and unconventional. We propose that our method allowed initial electrostatic interactions between chitosan and SP via thermomechanical mixing and subsequent hydrogen bonding and chitosan crystallization during conditioning, which are mainly responsible for the largely enhanced mechanical properties. These

interactions enabled excellent miscibility and compatibility between chitosan and SP as well as a strong, rigid, well-integrated structure in the alloy material.

The novel biopolymer alloy materials developed in this study will be highly beneficial for applications requiring exceptional mechanical properties, biocompatibility and biodegradability, such as various consumer products (e.g., packaging, disposable cups/bottles/containers) and biomedical materials (e.g., implants, tissue engineering scaffolds, drug delivery carriers). More importantly, our simple approach does not resort to complex chemistries and 3D-structural construction. This study is expected to open a new research direction in biopolymer processing for developing high-performance polymer materials where performance, cost-effectiveness and environmental sustainability are the research priorities of future industry.

ASSOCIATED CONTENT

Supporting Information (SI) is available free of charge on the ACS Publications website at DOI: xxx. See SI for supplementary Tables and Figure.

AUTHOR INFORMATION

Corresponding Author

* Fengwei Xie. Email: f.xie@uq.edu.au, fwhsieh@gmail.com

Author Contributions

The manuscript was written through contributions of all authors. All authors have given approval to the final version of the manuscript. ‡These authors contributed equally.

Notes

The authors declare no competing financial interest.

ACKNOWLEDGMENT

F. Xie acknowledges the European Union's Marie Skłodowska-Curie Actions (MSCA) and the Institute of Advanced Study (IAS), University of Warwick for the Warwick Interdisciplinary Research Leadership Programme (WIRL-COFUND).

ABBREVIATIONS

SF, silk fibroin; SP, silk peptide; RH, relative humidity; σ, Maximum tensile strength; ε_b, elongation at break; E, Young's modulus; U_T, toughness; FTIR, Fourier-transform

infrared; TGA, thermogravimetric analysis; DMTA, dynamic mechanical thermal analysis; XRD, X-ray diffraction; SEM, scanning electron microscope; WU, water update.

REFERENCES

(1) Rabea, E. I.; Badawy, M. E. T.; Stevens, C. V.; Smagghe, G.; Steurbaut, W. Chitosan as antimicrobial agent: Applications and mode of action. *Biomacromolecules* **2003,** *4* (6), 1457-1465, DOI: 10.1021/bm034130m.

(2) Kong, M.; Chen, X. G.; Xing, K.; Park, H. J. Antimicrobial properties of chitosan and mode of action: A state of the art review. *International Journal of Food Microbiology* **2010,** *144* (1), 51-63, DOI: http://dx.doi.org/10.1016/j.ijfoodmicro.2010.09.012.

(3) Badawy, M. E. I.; Rabea, E. I. A Biopolymer Chitosan and Its Derivatives as Promising Antimicrobial Agents against Plant Pathogens and Their Applications in Crop Protection. *International Journal of Carbohydrate Chemistry* **2011,** *2011*, DOI: 10.1155/2011/460381.

(4) Verlee, A.; Mincke, S.; Stevens, C. V. Recent developments in antibacterial and antifungal chitosan and its derivatives. *Carbohydr. Polym.* **2017,** *164*, 268-283, DOI: http://dx.doi.org/10.1016/j.carbpol.2017.02.001.

(5) Cado, G.; Aslam, R.; Séon, L.; Garnier, T.; Fabre, R.; Parat, A.; Chassepot, A.; Voegel, J. C.; Senger, B.; Schneider, F.; Frère, Y.; Jierry, L.; Schaaf, P.; Kerdjoudj, H.; Metz-Boutigue, M. H.; Boulmedais, F. Self-Defensive Biomaterial Coating Against Bacteria and Yeasts: Polysaccharide Multilayer Film with Embedded Antimicrobial Peptide. *Adv. Funct. Mater.* **2013,** *23* (38), 4801-4809, DOI: 10.1002/adfm.201300416.

(6) Wan Ngah, W. S.; Teong, L. C.; Hanafiah, M. A. K. M. Adsorption of dyes and heavy metal ions by chitosan composites: A review. *Carbohydr. Polym.* **2011,** *83* (4), 1446-1456, DOI:

http://dx.doi.org/10.1016/j.carbpol.2010.11.004.

(7) Gerente, C.; Lee, V. K. C.; Cloirec, P. L.; McKay, G. Application of chitosan for the removal of metals from wastewaters by adsorption—mechanisms and models review. *Critical Reviews in Environmental Science and Technology* **2007,** *37* (1), 41-127, DOI: 10.1080/10643380600729089.

(8) Guibal, E. Interactions of metal ions with chitosan-based sorbents: a review. *Sep. Purif. Technol.* **2004,** *38* (1), 43-74, DOI: http://dx.doi.org/10.1016/j.seppur.2003.10.004.

(9) Varma, A. J.; Deshpande, S. V.; Kennedy, J. F. Metal complexation by chitosan and its derivatives: a review. *Carbohydr. Polym.* **2004,** *55* (1), 77-93, DOI: http://dx.doi.org/10.1016/j.carbpol.2003.08.005.

(10) Zhang, S.; Lu, F.; Tao, L.; Liu, N.; Gao, C.; Feng, L.; Wei, Y. Bio-inspired anti-oil-fouling chitosan-coated mesh for oil/water separation suitable for broad ph range and hyper-saline environments. *ACS Appl. Mater. Interfaces* **2013,** *5* (22), 11971-11976, DOI: 10.1021/am403203q.

(11) You, J.; Li, M.; Ding, B.; Wu, X.; Li, C. Crab Chitin-Based 2D Soft Nanomaterials for Fully Biobased Electric Devices. *Adv. Mater.* **2017,** *17* (19), 1606895, DOI: 10.1002/adma.201606895.

(12) Lu, L.; Chen, W. Biocompatible Composite Actuator: A Supramolecular Structure Consisting of the Biopolymer Chitosan, Carbon Nanotubes, and an Ionic Liquid. *Adv. Mater.* **2010,** *22* (33), 3745-3748, DOI: 10.1002/adma.201001134.

(13) Wang, R.; Gao, S.; Yang, Z.; Li, Y.; Chen, W.; Wu, B.; Wu, W. Engineered and Laser‐Processed Chitosan Biopolymers for Sustainable and Biodegradable Triboelectric Power Generation. *Adv. Mater.* **2018,** *30* (11), 1706267, DOI: doi:10.1002/adma.201706267.

(14) Koh, L.-D.; Cheng, Y.; Teng, C.-P.; Khin, Y.-W.; Loh, X.-J.; Tee, S.-Y.; Low, M.; Ye, E.; Yu, H.-D.; Zhang, Y.-W.; Han, M.-Y. Structures, mechanical properties and applications of silk fibroin materials. *Progress in Polymer Science* **2015,** *46* (Supplement C), 86-110, DOI: https://doi.org/10.1016/j.progpolymsci.2015.02.001.

(15) Kundu, B.; Rajkhowa, R.; Kundu, S. C.; Wang, X. Silk fibroin biomaterials for tissue regenerations. *Adv. Drug Delivery Rev.* **2013,** *65* (4), 457-470, DOI: https://doi.org/10.1016/j.addr.2012.09.043.

(16) Zhou, Z.; Shi, Z.; Cai, X.; Zhang, S.; Corder, S. G.; Li, X.; Zhang, Y.; Zhang, G.; Chen, L.; Liu, M.; Kaplan, D. L.; Omenetto, F. G.; Mao, Y.; Tao, Z.; Tao, T. H. The Use of Functionalized Silk Fibroin Films as a Platform for Optical Diffraction-Based Sensing Applications. *Adv. Mater.* **2017**, 1605471-n/a, DOI: 10.1002/adma.201605471.

(17) Ling, S.; Wang, Q.; Zhang, D.; Zhang, Y.; Mu, X.; Kaplan, D. L.; Buehler, M. J. Integration of Stiff Graphene and Tough Silk for the Design and Fabrication of Versatile Electronic Materials. *Adv. Funct. Mater.* **2018,** *28* (9), 1705291, DOI: doi:10.1002/adfm.201705291.

(18) Wang, Q.; Jian, M.; Wang, C.; Zhang, Y. Carbonized Silk Nanofiber Membrane for Transparent and Sensitive Electronic Skin. *Adv. Funct. Mater.* **2017**, 1605657-n/a, DOI: 10.1002/adfm.201605657.

(19) Hu, K.; Gupta, M. K.; Kulkarni, D. D.; Tsukruk, V. V. Ultra-Robust Graphene Oxide-Silk Fibroin Nanocomposite Membranes. *Adv. Mater.* **2013,** *25* (16), 2301-2307, DOI: 10.1002/adma.201300179.

(20) Moo-Seok, H.; Gwang-Mun, C.; Joohee, K.; Jiuk, J.; Byeongwook, C.; Joong-Kwon, K.; Seunghwan, J.; Seongmin, L.; Hee-Young, K.; Hyun-Bin, H.; Hyeon-Gyun, I.; Jang-Ung, P.; Byeong-Soo, B.; Jungho, J. Biomimetic Chitin–Silk Hybrids: An Optically Transparent Structural Platform for Wearable Devices and Advanced Electronics. *Adv. Funct. Mater.* **2018,** *28* (24), 1705480, DOI: doi:10.1002/adfm.201705480.

(21) Kim, H. S.; Kim, J. T.; Jung, Y. J.; Ryu, S. C.; Son, H. J.; Kim, Y. G. Preparation of a porous chitosan/fibroin-hydroxyapatite composite matrix for tissue engineering. *Macromol. Res.* **2007,** *15* (1), 65-73, DOI: 10.1007/bf03218754.

(22) Wang, L.; Li, C. Preparation and physicochemical properties of a novel hydroxyapatite/chitosan–silk fibroin composite. *Carbohydr. Polym.* **2007,** *68* (4), 740-745, DOI: https://doi.org/10.1016/j.carbpol.2006.08.010.

(23) Chen, J.-P.; Chen, S.-H.; Lai, G.-J. Preparation and characterization of biomimetic silk fibroin/chitosan composite nanofibers by electrospinning for osteoblasts culture. *Nanoscale Research Letters* **2012,** *7* (1), 170, DOI: 10.1186/1556-276x-7-170.

(24) Lima, P. A. L.; Resende, C. X.; de Almeida Soares, G. D.; Anselme, K.; Almeida, L. E. Preparation,

characterization and biological test of 3D-scaffolds based on chitosan, fibroin and hydroxyapatite for bone tissue engineering. *Mater. Sci. Eng., C* **2013,** *33* (6), 3389-3395, DOI: https://doi.org/10.1016/j.msec.2013.04.026.

(25) Sionkowska, A.; Płanecka, A. Preparation and characterization of silk fibroin/chitosan composite sponges for tissue engineering. *J. Mol. Liq.* **2013,** *178* (Supplement C), 5-14, DOI: https://doi.org/10.1016/j.molliq.2012.10.042.

(26) Zeng, S.; Liu, L.; Shi, Y.; Qiu, J.; Fang, W.; Rong, M.; Guo, Z.; Gao, W. Characterization of Silk Fibroin/Chitosan 3D Porous Scaffold and In Vitro Cytology. *PLoS One* **2015,** *10* (6), e0128658, DOI: 10.1371/journal.pone.0128658.

(27) Vishwanath, V.; Pramanik, K.; Biswas, A. Optimization and evaluation of silk fibroin-chitosan freeze-dried porous scaffolds for cartilage tissue engineering application. *J. Biomater. Sci., Polym. Ed.* **2016,** *27* (7), 657-674, DOI: 10.1080/09205063.2016.1148303.

(28) Vincent, J. F. V.; Wegst, U. G. K. Design and mechanical properties of insect cuticle. *Arthropod Structure & Development* **2004,** *33* (3), 187-199, DOI: https://doi.org/10.1016/j.asd.2004.05.006.

(29) Meyers, M. A.; Chen, P.-Y.; Lin, A. Y.-M.; Seki, Y. Biological materials: Structure and mechanical properties. *Prog. Mater. Sci.* **2008,** *53* (1), 1-206, DOI: https://doi.org/10.1016/j.pmatsci.2007.05.002.

(30) Sanchez, C.; Arribart, H.; Giraud Guille, M. M. Biomimetism and bioinspiration as tools for the design of innovative materials and systems. *Nat. Mater.* **2005,** *4* (4), 277-288.

(31) Zhang, C.; McAdams, D. A.; Grunlan, J. C. Nano/Micro-Manufacturing of Bioinspired Materials: a Review of Methods to Mimic Natural Structures. *Adv. Mater.* **2016,** *28* (30), 6292-6321, DOI: 10.1002/adma.201505555.

(32) Ortiz, C.; Boyce, M. C. Bioinspired structural materials. *Science* **2008,** *319* (5866), 1053-1054, DOI: 10.1126/science.1154295.

(33) Fernandez, J. G.; Ingber, D. E. Unexpected strength and toughness in chitosan-fibroin laminates inspired by insect cuticle. *Adv. Mater.* **2012,** *24* (4), 480-484, DOI: 10.1002/adma.201104051.

(34) Nogueira, G. M.; Swiston, A. J.; Beppu, M. M.; Rubner, M. F. Layer-by-Layer Deposited

Chitosan/Silk Fibroin Thin Films with Anisotropic Nanofiber Alignment. *Langmuir* **2010,** *26* (11), 8953-8958, DOI: 10.1021/la904741h.

(35) Mekonnen, T.; Mussone, P.; Khalil, H.; Bressler, D. Progress in bio-based plastics and plasticizing modifications. *J. Mater. Chem. A* **2013,** *1* (43), 13379-13398, DOI: 10.1039/C3TA12555F.

(36) Chen, X.; Li, W.; Yu, T. Conformation transition of silk fibroin induced by blending chitosan. *J. Polym. Sci., Part B: Polym. Phys.* **1997,** *35* (14), 2293-2296, DOI: 10.1002/(SICI)1099-0488(199710)35:14<2293::AID-POLB9>3.0.CO;2-X.

(37) Chen, X.; Li, W.; Zhong, W.; Lu, Y.; Yu, T. pH sensitivity and ion sensitivity of hydrogels based on complex-forming chitosan/silk fibroin interpenetrating polymer network. *J. Appl. Polym. Sci.* **1997,** *65* (11), 2257-2262, DOI: 10.1002/(SICI)1097-4628(19970912)65:11<2257::AID-APP23>3.0.CO;2-Z.

(38) Kweon, H.; Um, I. C.; Park, Y. H. Structural and thermal characteristics of *Antheraea pernyi* silk fibroin/chitosan blend film. *Polymer* **2001,** *42* (15), 6651-6656, DOI: https://doi.org/10.1016/S0032-3861(01)00104-5.

(39) Sionkowska, A.; Płanecka, A. Surface properties of thin films based on the mixtures of chitosan and silk fibroin. *J. Mol. Liq.* **2013,** *186* (Supplement C), 157-162, DOI: https://doi.org/10.1016/j.molliq.2013.07.008.

(40) Kweon, H.; Ha, H. C.; Um, I. C.; Park, Y. H. Physical properties of silk fibroin/chitosan blend films. *J. Appl. Polym. Sci.* **2001,** *80* (7), 928-934, DOI: 10.1002/app.1172.

(41) Sionkowska, A.; Lewandowska, K.; Płanecka, A. Miscibility and physical properties of chitosan and silk fibroin mixtures. *J. Mol. Liq.* **2014,** *198* (Supplement C), 354-357, DOI: https://doi.org/10.1016/j.molliq.2014.07.033.

(42) Song, J.; Chen, C.; Zhu, S.; Zhu, M.; Dai, J.; Ray, U.; Li, Y.; Kuang, Y.; Li, Y.; Quispe, N.; Yao, Y.; Gong, A.; Leiste, U. H.; Bruck, H. A.; Zhu, J. Y.; Vellore, A.; Li, H.; Minus, M. L.; Jia, Z.; Martini, A.; Li, T.; Hu, L. Processing bulk natural wood into a high-performance structural material. *Nature* **2018,** *554*, 224, DOI: 10.1038/nature25476 https://www.nature.com/articles/nature25476#supplementary-information.

(43) Yang, X.; Liu, G.; Peng, L.; Guo, J.; Tao, L.; Yuan, J.; Chang, C.; Wei, Y.; Zhang, L. Highly Efficient Self-Healable and Dual Responsive Cellulose-Based Hydrogels for Controlled Release and 3D Cell Culture. *Adv. Funct. Mater.* **2017,** *27* (40), 1703174-n/a, DOI: 10.1002/adfm.201703174.

(44) Wu, G.; Chan, K.-C.; Zhu, L.; Sun, L.; Lu, J. Dual-phase nanostructuring as a route to high-strength magnesium alloys. *Nature* **2017,** *545*, 80, DOI: 10.1038/nature21691 https://www.nature.com/articles/nature21691#supplementary-information.

(45) Luo, S.; Cao, J.; McDonald, A. G. Interfacial Improvements in a Green Biopolymer Alloy of Poly(3-hydroxybutyrate-co-3-hydroxyvalerate) and Lignin via in Situ Reactive Extrusion. *ACS Sustainable Chemistry & Engineering* **2016,** *4* (6), 3465-3476, DOI: 10.1021/acssuschemeng.6b00495.

(46) Xu, D.; Huang, J.; Zhao, D.; Ding, B.; Zhang, L.; Cai, J. High-Flexibility, High-Toughness Double-Cross-Linked Chitin Hydrogels by Sequential Chemical and Physical Cross-Linkings. *Adv. Mater.* **2016,** *28* (28), 5844-5849, DOI: 10.1002/adma.201600448.

(47) Zhao, D.; Huang, J.; Zhong, Y.; Li, K.; Zhang, L.; Cai, J. High-Strength and High-Toughness Double-Cross-Linked Cellulose Hydrogels: A New Strategy Using Sequential Chemical and Physical Cross-Linking. *Adv. Funct. Mater.* **2016,** *26* (34), 6279-6287, DOI: 10.1002/adfm.201601645.

(48) Ye, D.; Cheng, Q.; Zhang, Q.; Wang, Y.; Chang, C.; Li, L.; Peng, H.; Zhang, L. Deformation Drives Alignment of Nanofibers in Framework for Inducing Anisotropic Cellulose Hydrogels with High Toughness. *ACS Appl. Mater. Interfaces* **2017,** *9* (49), 43154-43162, DOI: 10.1021/acsami.7b14900.

(49) Jones, O. G.; McClements, D. J. Recent progress in biopolymer nanoparticle and microparticle formation by heat-treating electrostatic protein–polysaccharide complexes. *Adv. Colloid Interface Sci.* **2011,** *167* (1), 49-62, DOI: https://doi.org/10.1016/j.cis.2010.10.006.

(50) Turgeon, S. L.; Schmitt, C.; Sanchez, C. Protein–polysaccharide complexes and coacervates. *Curr. Opin. Colloid Interface Sci.* **2007,** *12* (4), 166-178, DOI: https://doi.org/10.1016/j.cocis.2007.07.007.

(51) Rinaudo, M. Main properties and current applications of some polysaccharides as biomaterials. *Polym. Int.* **2008,** *57* (3), 397-430, DOI: 10.1002/pi.2378.

(52) Xie, D. F.; Martino, V. P.; Sangwan, P.; Way, C.; Cash, G. A.; Pollet, E.; Dean, K. M.; Halley, P. J.;

Avérous, L. Elaboration and properties of plasticised chitosan-based exfoliated nano-biocomposites. *Polymer* **2013,** *54* (14), 3654-3662, DOI: 10.1016/j.polymer.2013.05.017.

(53) Ritchie, R. O. The conflicts between strength and toughness. *Nat. Mater.* **2011,** *10*, 817, DOI: 10.1038/nmat3115.

(54) Wang, Y.; Chen, M.; Zhou, F.; Ma, E. High tensile ductility in a nanostructured metal. *Nature* **2002,** *419*, 912, DOI: 10.1038/nature01133 https://www.nature.com/articles/nature01133#supplementary-information.

(55) Sionkowska, A.; Płanecka, A.; Lewandowska, K.; Michalska, M. The influence of UV-irradiation on thermal and mechanical properties of chitosan and silk fibroin mixtures. *Journal of Photochemistry and Photobiology B: Biology* **2014,** *140* (Supplement C), 301-305, DOI: https://doi.org/10.1016/j.jphotobiol.2014.08.017.

(56) Frey, M.; Widner, D.; Segmehl, J. S.; Casdorff, K.; Keplinger, T.; Burgert, I. Delignified and Densified Cellulose Bulk Materials with Excellent Tensile Properties for Sustainable Engineering. *ACS Appl. Mater. Interfaces* **2018,** *10* (5), 5030-5037, DOI: 10.1021/acsami.7b18646.

(57) Shang, S.; Zhu, L.; Fan, J. Intermolecular interactions between natural polysaccharides and silk fibroin protein. *Carbohydr. Polym.* **2013,** *93* (2), 561-573, DOI: https://doi.org/10.1016/j.carbpol.2012.12.038.

(58) Basu, S.; Plucinski, A.; Catchmark, J. M. Sustainable barrier materials based on polysaccharide polyelectrolyte complexes. *Green Chem.* **2017,** *19* (17), 4080-4092, DOI: 10.1039/C7GC00991G.

(59) Hawley, T. G.; Johnson, T. B. The Isoelectric Point of Silk Fibroin. *Industrial & Engineering Chemistry* **1930,** *22* (3), 297-299, DOI: 10.1021/ie50243a023.

(60) Martino, V.; Pollet, E.; Avérous, L. Novative biomaterials based on chitosan and poly(ε-caprolactone): Elaboration of porous structures. *J. Polym. Environ.* **2011,** *19* (4), 819-826, DOI: 10.1007/s10924-011-0354-9.

(61) Epure, V.; Griffon, M.; Pollet, E.; Avérous, L. Structure and properties of glycerol-plasticized chitosan obtained by mechanical kneading. *Carbohydr. Polym.* **2011,** *83* (2), 947-952, DOI:

10.1016/j.carbpol.2010.09.003.

(62) Matet, M.; Heuzey, M.-C.; Pollet, E.; Ajji, A.; Avérous, L. Innovative thermoplastic chitosan obtained by thermo-mechanical mixing with polyol plasticizers. *Carbohydr. Polym.* **2013,** *95* (1), 241-251, DOI: 10.1016/j.carbpol.2013.02.052.

(63) Kittur, F. S.; Vishu Kumar, A. B.; Tharanathan, R. N. Low molecular weight chitosans—preparation by depolymerization with Aspergillus niger pectinase, and characterization. *Carbohydr. Res.* **2003,** *338* (12), 1283-1290, DOI: 10.1016/s0008-6215(03)00175-7.

(64) Takahashi, Y.; Gehoh, M.; Yuzuriha, K. Structure refinement and diffuse streak scattering of silk (*Bombyx mori*). *Int. J. Biol. Macromol.* **1999,** *24* (2), 127-138, DOI: https://doi.org/10.1016/S0141-8130(98)00080-4.

(65) Phillips, D. M.; Drummy, L. F.; Conrady, D. G.; Fox, D. M.; Naik, R. R.; Stone, M. O.; Trulove, P. C.; De Long, H. C.; Mantz, R. A. Dissolution and regeneration of *bombyx mori* silk fibroin using ionic liquids. *J. Am. Chem. Soc.* **2004,** *126* (44), 14350-14351, DOI: 10.1021/ja046079f.

(66) Brugnerotto, J.; Lizardi, J.; Goycoolea, F. M.; Argüelles-Monal, W.; Desbrières, J.; Rinaudo, M. An infrared investigation in relation with chitin and chitosan characterization. *Polymer* **2001,** *42* (8), 3569-3580, DOI: https://doi.org/10.1016/S0032-3861(00)00713-8.

(67) Sannan, T.; Kurita, K.; Ogura, K.; Iwakura, Y. Studies on chitin: 7. I.r. spectroscopic determination of degree of deacetylation. *Polymer* **1978,** *19* (4), 458-459, DOI: https://doi.org/10.1016/0032-3861(78)90256-2.

(68) Tsukada, M.; Gotoh, Y.; Nagura, M.; Minoura, N.; Kasai, N.; Freddi, G. Structural changes of silk fibroin membranes induced by immersion in methanol aqueous solutions. *J. Polym. Sci., Part B: Polym. Phys.* **1994,** *32* (5), 961-968, DOI: 10.1002/polb.1994.090320519.

(69) Kweon, H. Y.; Um, I. C.; Park, Y. H. Thermal behavior of regenerated *Antheraea pernyi* silk fibroin film treated with aqueous methanol. *Polymer* **2000,** *41* (20), 7361-7367, DOI: https://doi.org/10.1016/S0032-3861(00)00100-2.

(70) Canetti, M.; Seves, A.; Secundo, F.; Vecchio, G. CD and small-angle x-ray scattering of silk fibroin

in solution. *Biopolymers* **1989,** *28* (9), 1613-1624, DOI: 10.1002/bip.360280910.

(71) Iizuka, E.; Yang, J. T. The disordered and -conformations of silk fibroin in solution. *Biochemistry* **1968,** *7* (6), 2218-2228, DOI: 10.1021/bi00846a026.

(72) Quijada-Garrido, I.; Laterza, B.; Mazón-Arechederra, J. M.; Barrales-Rienda, J. M. Characteristic Features of Chitosan/Glycerol Blends Dynamics. *Macromol. Chem. Phys.* **2006,** *207* (19), 1742-1751, DOI: 10.1002/macp.200600230.

(73) Quijada-Garrido, I.; Iglesias-González, V.; Mazón-Arechederra, J. M.; Barrales-Rienda, J. M. The role played by the interactions of small molecules with chitosan and their transition temperatures. Glass-forming liquids: 1,2,3-Propantriol (glycerol). *Carbohydr. Polym.* **2007,** *68* (1), 173-186, DOI: 10.1016/j.carbpol.2006.07.025.

(74) Motta, A.; Fambri, L.; Migliaresi, C. Regenerated silk fibroin films: Thermal and dynamic mechanical analysis. *Macromol. Chem. Phys.* **2002,** *203* (10-11), 1658-1665, DOI: 10.1002/1521-3935(200207)203:10/11<1658::AID-MACP1658>3.0.CO;2-3.

(75) Tsukada, M.; Obo, M.; Kato, H.; Freddi, G.; Zanetti, F. Structure and dyeability of Bombyx mori silk fibers with different filament sizes. *Journal of Applied Polymer Science* **1996,** *60* (10), 1619-1627, DOI: 10.1002/(SICI)1097-4628(19960606)60:10<1619::AID-APP14>3.0.CO;2-#.

- Table of Contents -

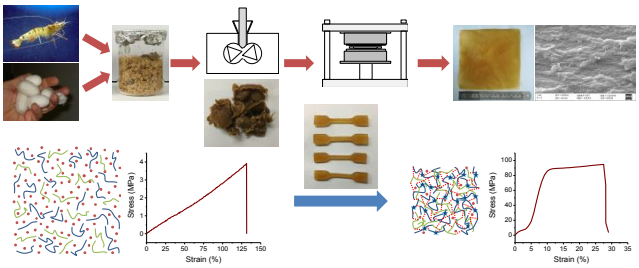

Ultrastrong chitosan–silk peptide alloy films are fabricated by a facile, “dry” process, leading to cost-effective utilization of sustainable resources.